Models of stress fluctuations in granular media

P. Claudin and J.-P. Bouchaud
Service de Physique de l'Etat Condensé, CEA, Orme des Merisiers, 91191 Gif-sur-Yvette, Cedex, France

M. E. Cates and J. P. Wittmer
Department of Physics and Astronomy, JCMB King's Buildings, University of Edinburgh, Mayfield Road, Edinburgh EH9 3JZ, United Kingdom

(Received 19 November 1997)

We investigate in detail two models describing how stresses propagate and fluctuate in granular media. The first one is a scalar model where only the vertical component of the stress tensor is considered. In the continuum limit, this model is equivalent to a *diffusion equation* (where the role of time is played by the vertical coordinate) plus a randomly varying convection term. We calculate the response and correlation function of this model and discuss several properties, in particular related to the stress distribution function. We then turn to the tensorial model, where the basic starting point is a wave equation that, in the absence of disorder, leads to a raylike propagation of stress. In the presence of disorder, the rays acquire a diffusive width and the angle of propagation is shifted. A striking feature is that the response function becomes negative, which suggests that the contact network is mechanically unstable to very weak perturbations. The stress correlation function reveals characteristic features related to the raylike propagation, which are absent in the scalar description. Our analytical calculations are confirmed and extended by a numerical analysis of the stochastic wave equation. [S1063-651X(98)07004-4]

PACS number(s): 81.05.Rm, 46.10.+z, 05.40.+j, 83.70.Fn

I. INTRODUCTION

Granular media are materials where stress fluctuations are large, even on scales much larger than the grain size. Repeatedly pouring the very same amount of powder in a silo results in fluctuations of the weight supported by the bottom plate of 20% or more [1,2]. This weight furthermore changes very abruptly when temperature changes by only a few degrees Celsius, which induces only very small changes of the size of each grain [2,3].

More quantitative experiments were recently performed by Liu *et al.* [4], Brockbank, Huntley, and Ball [5], and Mueth, Jaeger, and Nagel [6], where the local fluctuations of the normal stress deep inside a silo or at the base of a sandpile were measured (see also [7] and for early qualitative experiments [8]). It was found that the stress probability distribution is rather broad (i.e., the relative fluctuations are of order one), decaying exponentially for large stresses. A simple ''scalar'' model for stress propagation was introduced and studied in detail [4,9], which predicts a stress probability distribution in good agreement with experimental (and numerical) data. However, this model considers only the *vertical* normal component of the stress tensor and discards all the other components: In this sense the model is scalar.

A fully ''tensorial'' model for stress propagation in homogeneous granular media was proposed in [10–12] to account for the pressure ''dip'' that is observed experimentally below the apex of conical sandpiles. The most striking feature of this model is that the stress propagation equation is a *wave equation*, with the vertical axis playing the role of time. Correspondingly, the stress propagates (in two dimensions; see [10]) along two rays, which makes a certain angle with the vertical axis (the ''light cone''). This must be contrasted with the scalar model, where stresses travel essentially vertically, which predicts a central pressure ''hump'' (rather than a dip).

It is thus *a priori* not obvious that the scalar model is a suitable starting point for the description of fluctuations. Conversely, the influence of local randomness within the tensorial model was not yet investigated and is very interesting *per se*. In particular, it is important to know if and how the idea of a light cone survives in the presence of disorder and how the stress fluctuations develop.

The aim of the present paper is to calculate analytically (in two dimensions) the average response function (Green's function) and the two-point correlation function for the tensorial model in the presence of disorder and to compare the results with those obtained within a scalar description. We find that the cone survives at small disorder (although the cone angle is shifted and acquires a nonzero width, which we compute). More surprisingly, the Green's function takes *negative values*, a feature that we checked numerically, which we discuss in detail in terms of the essential ''fragility'' of the contact network. (That the Green's function can take negative values in the presence of inhomogeneities was already noticed within the fixed principal axis (FPA) model in [12].) We show that the two-point correlation function keeps a signature of this conelike propagation. For large disorder, however, the theory suggests that the structure of the large-scale equations could change drastically, from a *hyperbolic* wave equation to an *elliptic* equation, akin to (but distinct from) those appearing in elasticity theory. The interpretation of the equations, however, suggests that by the time this happens, the pile is unstable to any perturbations and spontaneously rearranges.

The tensorial stress probability distribution is investigated numerically, with certain results that are close to those of the scalar model. We explain this by showing that a special case

of the tensorial model actually reduces to the superposition of *two* independent scalar models.

This paper is constructed as follows. In Sec. II we review the properties of the scalar model, including results that appeared in the literature in very different contexts (scalar diffusion in turbulence and localization). In Sec. III the random wave equation for the tensorial case is motivated by a microscopic model and simulations and studied using perturbation theory in the strength of the disorder. We discuss how the line shape of the response function distorts from two δ peaks to (eventually) one broad peak as disorder increases. Some generalizations of the random wave equation are considered in Sec. IV. In Sec. V we present numerical results for the stress distribution function and compare them with the predictions of the scalar model and also of direct simulations of sphere packings [13,14]. We discuss a limit where the two models can be quantitatively compared. Finally, in Sec. VI a summary of the most interesting results is given, with suggestions of future experiments and open questions.

II. THE SCALAR MODEL

A. The discrete version

1. Definition

The main assumption of the scalar model is that only the vertical normal component of the stress tensor $w=\sigma_{zz}$ (the ''weight'') needs to be considered. If the grains reside on the nodes of a two-dimensional lattice (see Fig. 1), the simplest model for weight propagation down the pile is

$$w(i,j)=w_g+q_+(i-1,j-1)w(i-1,j-1)+q_-(i+1,j-1)w(i+1,j-1), \tag{1}$$

where w_g is the weight of each grain and $q_\pm(i,j)$ are ''transmission'' coefficients giving the fraction of weight that the grain (i,j) transmits to its right (left) neighbor immediately below. Mass conservation imposes that $q_+(i,j)+q_-(i,j)=1$ for all i,j. The case of an ordered pile of identical grains would correspond to $q_\pm=\frac{1}{2}$. The authors of [4,9] proposed to take into account (in a phenomenological way) the local disorder in packing, grain sizes, shapes, etc., by choosing $q_+(i,j)$ to be independent random numbers (except for the above constraint), for example, uniformly distributed between 0 and 1. This model, which we shall call the Liu *et al.* model (or q model), was originally written with an arbitrary number N of downward neighbors ($N=2$ in the example above) and can thus be (in principle) generalized to three dimensions.

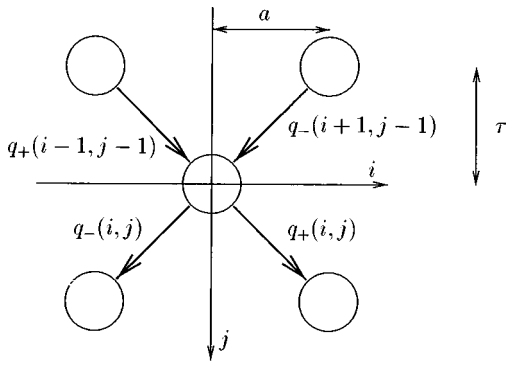

FIG. 1. The Liu *et al.* model with two neighbors. $q_\pm$'s are independent random variables, except for the weight conservation constraint $q_+(i,j)+q_-(i,j)=1$.

2. Results on the stress distribution: Universality?

The case of a uniform distribution of the q's is interesting because it leads to an exact solution for the local weight distribution $P(w)$. In this limit, the correlation between two neighboring sites at the same altitude j is zero for all j. For more general q distributions, this is true only when j is large (see below). Thus $P(w)$ obeys the mean-field equation

$$P_{j+1}(w)=\int_0^1 dq_1 dq_2 \rho(q_1)\rho(q_2)\int_0^\infty dw_1 dw_2 \times P_j(w_1)P_j(w_2)\delta(w-(w_1q_1+w_2q_2+w_0)), \tag{2}$$

where $\rho(q)$ is the distribution of q, here taken to be $\rho(q)=1$. In the limit $j\to\infty$, the stationary distribution P^* of this equation is given by

$$P^*(w)=\frac{w}{W^2}\exp\left(-\frac{w}{W}\right), \tag{3}$$

where $2W=jw_g$ is the average weight. For $N\neq 2$, the distribution is instead a Γ distribution of parameter N; its small-w behavior is w^{N-1}, while the large-w tail is exponential. Liu *et al.* [4,9] have argued that this behavior is generic: For example, the condition for the local weight w to be small is that all the N q's reaching this site are themselves small; the phase-space volume for this is proportional to w^{N-1} if the distribution $\rho(q)$ is regular around $q=0$. However, if instead $\rho(q)\propto q^{\gamma-1}$ when q is small, one expects $P^*(w)$ to behave for small w as $w^{-\alpha}$, with $\alpha=1-N\gamma<0$. Similarly, the exponential tail at large w is sensitive to the behavior of $\rho(q)$ around $q=1$. In particular, if the maximum value of q is $q_M<1$, one can easily show by taking the Laplace transform of Eq. (2) that $P^*(w)$ decays *faster* than an exponential:

$$\ln P^*(w) \underset{w\to\infty}{\propto} -w^\beta \quad \text{with} \quad \beta=\frac{\ln N}{\ln(Nq_M)}. \tag{4}$$

(Notice that $\beta=1$ whenever $q_M=1$ and that $\beta\to\infty$ when $q_M=1/N$.)

In this sense, the exponential tail of $P^*(w)$ is not universal: It requires the possibility that one of the q can be arbitrarily close to 1. This implies that all other q's originating from that point are close to zero, i.e., that there is a nonzero probability density that one grain is entirely bearing on one of its downward neighbors.

Note that if q can only take the values 0 or 1, the distribution $P(w)$ becomes a power law $P^*(w)\propto w^{-\alpha}$, with $\alpha=4/3$ for $N=2$ [9]. This power law is, however, truncated for large w as soon as values for q different from 0 and 1 are allowed.

How well does the simple distribution (3) compare to experiments and numerical simulations? The exponential decay for large w appears in some cases to overestimate both the

experimental [5] and numerical tail [4] (see also Sec. V), suggesting a value of β somewhat larger than 1. On the other hand, the probability to observe very small w is very underestimated by Eq. (3): See [5,13,6] and Sec. V. This might be due to the fact that *arching* effects are absent in this scalar model. A generalization of the Liu *et al.* model allowing for arching was suggested in [3], which generates sites where $q_+=1$ and $q_-=0$ (or vice versa). This indeed leads to much higher probability density for small weights, $P^*(w)\propto w^{-\alpha}$, as argued in [9]; see also [15].

B. Continuous limit of the scalar model

Let us focus on the case $N=2$ and define v to be such that $q_\pm(i,j)=[1\pm v(i,j)]/2$. If v is small, the local weight is smoothly varying and the discrete equation (1) can then be written in the differential form

$$\partial_t w+\partial_x(v w)=\rho+D_0\partial_{xx}w, \tag{5}$$

where $x=ia$ and $t=j\tau$ are the horizontal and (downward) vertical variables corresponding to indices i and j of Fig. 1 and a and τ are of the order of the size of the grains. The vertical coordinate has been called t for its obvious analogy with time in a diffusion problem. ρ is the density of the material (the gravity g is taken to be equal to 1) and D_0 a ''diffusion'' constant, which depends on the geometry of the lattice on which the discrete model has been defined. For a rectangular lattice as shown in Fig. 1, $D_0=a^2/2\tau$. More generally, the diffusion constant is of the order of magnitude of the size of the grains a.

In this model and in the following, we shall assume that the density ρ is not fluctuating. Density fluctuations could be easily included; it is, however, easy to understand that the resulting relative fluctuations of the weight at the bottom of the pile decrease with the height of the pile H as $H^{-1/2}$ and are thus much smaller than those induced by the randomly fluctuating direction of propagation, encoded by q (or v), which remain of order 1 as $H\to\infty$. Two interesting quantities to compute are the average ''response'' $G(x,t|x_0,t_0)$ to a small density change at point (x_0,t_0), measured at point (x,t), and the correlation function of the force field $C(x,t,x',t')=\langle w(x,t)w(x',t')\rangle_c$ (connected part), where the averaging is taken over the realization of the noise $v(x,t)$.

Equation (5) shows that the scalar model of stress propagation is identical to that describing tracer diffusion in a (time-dependent) flow $v(x,t)$. This problem has been the subject of many recent works in the context of turbulence [16,17]; we believe that interesting qualitative analogies with that field can be made. In particular, ''intermittent'' bunching of the tracer field corresponds in the present context to patches of large stresses, which may induce anomalous scaling for higher moments of the stress field correlation function. We refer the reader to [16,17] for further details.

1. Statistics of the noise $v(x,t)$

The noise term v represents the effect of local heterogeneities in the granular packing. Its mean value is taken to be zero and its correlation function is chosen for simplicity to be of the factorable form $\langle v(x,t)v(x',t')\rangle=\sigma^2 g_x(x-x')g_t(t-t')$, where g_x and g_t are noise correlation functions along the x and t axes. We shall take g_x and g_t to be short ranged (although this may not be justified; fluctuations in the microstructure of granular media may turn out to be long-ranged due to, e.g., the presence of long stress paths or arches), with correlation lengths ℓ_x and ℓ_t. Our aim is to describe the system at a scale L much larger than both the lattice and the correlation lengths: $a,\tau,\ell_x,\ell_t\ll L$. This will allow us to look for solutions in the regime $k,E\to 0$, where k and E are the conjugate variables for x and t, respectively, in Fourier-Laplace space. However, we shall see below that the limit $a,\tau,\ell_x,\ell_t\to 0$ can be tricky and must be treated with care: This is because the noise appears in a multiplicative manner in Eq. (5). (In the tensorial case, the limit $\ell_t\to 0$ actually makes the problem trivial, for a reason that will become clear below.) For computational purposes, we shall often implicitly assume that the probability distribution of v is Gaussian; this might, however, introduce artifacts, which we discuss.

2. Fourier transforms

The limit where $a,\ell_x\to 0$ is ill defined and leads to a divergence of the perturbation theory in σ for large wave vectors k. We thus choose to regularize the problem by working within the first Brillouin zone, i.e., we keep all wave-vector components within the interval $\mathcal{I}=[-\Lambda,+\Lambda]$, where $\Lambda=\pi/a$. Our Fourier conventions for a given quantity f will then be

$$f(x,t)=\int_{-\Lambda}^{\Lambda}\frac{dk}{2\pi}\,e^{ikx}f(k,t), \tag{6}$$

$$f(k,t)=\ell_x\sum_{x=-\infty}^{+\infty}e^{-ikx}f(x,t). \tag{7}$$

One has to be particularly careful when computing convolution integrals, such as $\int(dq/2\pi)f_1(q)f_2(k-q)$, which must be understood with limits $-\Lambda+k$ and Λ ($-\Lambda$ and $\Lambda+k$) if $k\geqslant 0$ ($k\leqslant 0$). An important example, which will appear in the response function calculations, is

$$\int_{q,k-q\in\mathcal{I}}\frac{dq}{2\pi}\,q=\frac{\Lambda k}{2\pi}+O(k^2). \tag{8}$$

Let us then take the Fourier transform of Eq. (5) along x, to obtain

$$(\partial_t+D_0k^2)w_k=\rho_k+ik\int\frac{dq}{2\pi}\,w_q v_{k-q}. \tag{9}$$

Our aim is to calculate, in the small-k limit, the average response (or Green's) function $G(k,t-t')$, defined as the expectation value of the functional derivative $\langle\delta w(k,t)/\delta\rho(k,t')\rangle$, and the two-point correlation function of w, $\langle w(k,t)w(k',t)\rangle\equiv 2\pi\delta(k+k')C(k,t)$.

3. The noiseless Green's function

The noiseless (bare) Green's function (or ''propagator'') G_0 is the solution of the equation where the ''velocity'' components v_q are identically zero, $(\partial_t + D_0 k^2) G_0(k,t-t') = \delta(t-t')$, which is

$$G_0(k,t-t') = \theta(t-t') e^{-D_0 k^2 (t-t')} \tag{10}$$

or, in real space,

$$G_0(x,t-t') = \frac{\theta(t-t')}{\sqrt{4\pi D_0 (t-t')}} e^{-x^2/4D_0(t-t')}. \tag{11}$$

4. Ambiguities due to multiplicative noise: Ito vs Stratonovitch

In Eq. (9) we have omitted to specify the dependence on the variable t. There is actually an ambiguity in the product term $w_q v_{k-q}$. In the discrete Liu *et al.* model [4], the $q_\pm$'s emitted from a given site are independent of the value of the weight on that site. In the continuum limit, this corresponds to choosing $w_q(t)$ to be independent of $v_{k-q}(t)$ or that the v's must be thought of as slightly posterior to the w's [i.e., the product is read as $w_q(t-0) v_{k-q}(t+0)$]. In this case, the average of Eq. (9) is trivial and coincides with the noiseless limit; hence $G = G_0$. This can be understood directly on the discrete model by noticing that the Green's function $G(i,j|0,0)$ can be expressed as a sum over paths, all starting at site (0,0), and ending at site (i,j):

$$G(i,j|0,0) = \sum_{\text{paths } \mathcal{P}} \prod_{(k,l)\in\mathcal{P}} q_\pm(k,l), \tag{12}$$

where the $q_\pm(k,l)$ are either $q_+(k,l)$ or $q_-(k,l)$, depending on the path. Since each bond $q_\pm(k,l)$ appears only once in the product, the averaging over q is trivial and leads to

$$G(i,j|0,0) = \sum_{\text{paths } \mathcal{P}} 2^{-j} \equiv G_0(i,j|0,0). \tag{13}$$

(Note that this argument fails for the computation of the correlation function C since paths can ''interfere.'' We shall return later to this calculation.)

The above choice corresponds to Ito's prescription in stochastic calculus. Another choice (i.e., Stratonovitch's prescription) is possible, however, which corresponds to the proper continuum time limit in the case where the correlation length ℓ_t is very small, but not smaller than a (see Fig. 2). In this case, the w's and the v's cannot be taken to be independent. This is the choice that we shall make in the following.

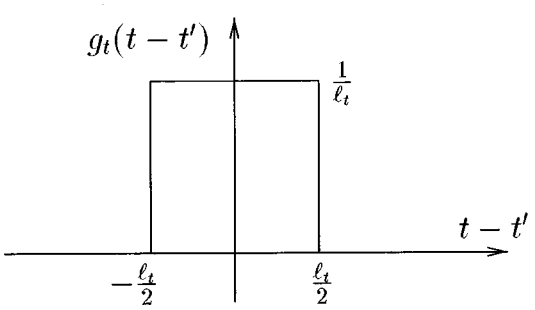

FIG. 2. Correlation function of the noise along t axis. The results presented below would hold for an arbitrary, symmetric, short-range function.

C. Calculation of the average response and correlation functions

Two approaches will be presented. The first one, based on Novikov's theorem, leads to exact (in the small-k limit) differential equations for G and C, which can be fully solved. The second one is a mode-coupling approximation (MCA), based on a resummation of perturbation theory. It happens that, for this particular model where the noise is Gaussian and short-range correlated in time, both approaches give the same results because perturbation theory is trivial. In other cases, though, where exact solutions are no longer available, the MCA is in general very useful to obtain nonperturbative results (see [18]). We shall see that the effect of the noise is to widen the diffusion peak: D_0 is renormalized by an additional term proportional to the variance of the noise v.

1. Novikov's theorem: Exact equations for G

Novikov's theorem provides the following identity, valid if the v are Gaussian random variables:

$$\langle w(k,t) v(k',t) \rangle = \int_0^t dt' \int \frac{dq}{2\pi} \left\langle \frac{\delta w(k,t)}{\delta v(q,t')} \right\rangle \times \langle v(q,t') v(k',t) \rangle. \tag{14}$$

Such a term actually appears in Eq. (9), after transformation into an equation for G:

$$(\partial_t + D_0 k^2) G(k,t-t') = \delta(t-t') - ik \frac{\delta}{\delta \rho(k,t')} \times \int \frac{dq}{2\pi} \langle v(q,t) w(k-q,t) \rangle. \tag{15}$$

In the limit where $\ell_x = a \to 0$, the noise correlation is of the form $\langle v(q,t) v(q',t') \rangle = 2\pi\sigma^2 \delta(q+q') \tilde{g}_x(q) g_t(t-t')$, with g_t peaked in $t=t'$ such that $f(t') g_t(t-t') \simeq f(t) g_t(t-t')$ for any function f. In all of Sec. II we take $\tilde{g}_x(q) = 1$. From formally integrating Eq. (9) between t' and t, one can express the equal-time derivative $\delta w / \delta v$ as

$$\left. \frac{\delta w(k,t)}{\delta v(k',t')} \right|_{t'=t-0} = -ikw(k-k',t) \tag{16}$$

and thus obtain

$$(\partial_t + D_0 k^2) G(k,t-t') = \delta(t-t') - \sigma^2 k G(k,t-t') \times \int_0^t dt' g_t(t-t') \int \frac{dq}{2\pi} (k-q). \tag{17}$$

Using the shape of the function g_t (see Fig. 2), the first integral is $\frac{1}{2}$. The second one is a convolution integral and its value is $\Lambda k/2\pi + O(k^2)$ [see Eq. (8)]. The final differential

equation for G is then, in the small-k limit, a diffusion equation with a renormalized diffusion constant

$$D_R = D_0 + \frac{\sigma^2 \Lambda}{4\pi}. \tag{18}$$

It is interesting to note that the model remains well defined in the limit where the ''bare'' diffusion constant is zero since a nonzero diffusion constant is induced by the fluctuating velocity v. This would not be true if Eq. (5) was interpreted with the Ito convention, where the fluctuating velocity would *not* lead to any spreading of the average density.

The most important conclusion is thus that, in the present scalar model, stresses propagates essentially vertically: Taking $\ell \sim a$, the response at depth H to a small perturbation is confined within a distance proportional to $\sqrt{D_R H}$ from the vertical. Since $D_R \simeq \ell^2/a$, $\sqrt{D_R H}$ is much less than H in the limit where $H \gg \ell^2/a$, i.e., when the height of the assembly of grains is much larger than the grain size.

2. Exact equations for C

Exact equations can also be derived for C in the limit $k \to 0$, following very similar calculations. From Eq. (9) one can deduce the corresponding one for $w(k,t)w(-k,t)$. Upon averaging, Novikov's theorem has to be used on quantities such as $\langle w(k,t)v(q,t)w(-k-q,t)\rangle$, finally leading to

$$(\partial_t + 2D_R k^2) C(k,t) = \sigma^2 k^2 \int \frac{dq}{2\pi} C(q,t). \tag{19}$$

One can formally integrate Eq. (19). It gives

$$C(k,t) = C(k,0) e^{-2D_R k^2 t} + \sigma^2 k^2 \int_0^t dt' e^{-2D_R k^2 (t-t')} \tilde{C}(t'), \tag{20}$$

where $\tilde{C}(t') = \int (dk/2\pi) C(k,t')$. Let us specify at this stage two specific initial conditions $C(k,0)$ that can be of interest. We consider, for simplicity, a random packing of ''table tennis'' balls with no mass ($\rho = 0$), but subject to a random overload of zero mean ($\langle w(x,0)w(x',0)\rangle = A_0^2 \delta(x-x')$) or to a constant overload [$w(x,t=0) = B_0$]. Therefore, $C(k,0) = A_0^2$ in the first case and $C(k,0) = B_0^2 \delta(k)$ in the second one. Equation (20) is then solved in two steps. We first integrate it over k and find a closed equation for $\tilde{C}$, which can be solved in Laplace transform. [Note that this is an approximation, since Eq. (20) is only valid for $k \to 0$.] We call E the conjugate variable of t. From $\tilde{C}(E)$, we get $\tilde{C}(t)$ and then finally compute $C(x,t)$.

(a) Random overload. In the small-E (large-t) limit, we get $\tilde{C}(E) \sim 1/\sqrt{E}$, meaning $\tilde{C}(t) = a_0/\sqrt{t}$, with

$$a_0 = \frac{D_R}{2D_0 - D_R} \frac{A_0}{\sqrt{8\pi D_R}}.$$

It finally leads to the following expression for $B(x,t) \equiv C(0,t) - C(x,t) = \frac{1}{2}\langle [w(x,t) - w(0,t)]^2 \rangle$:

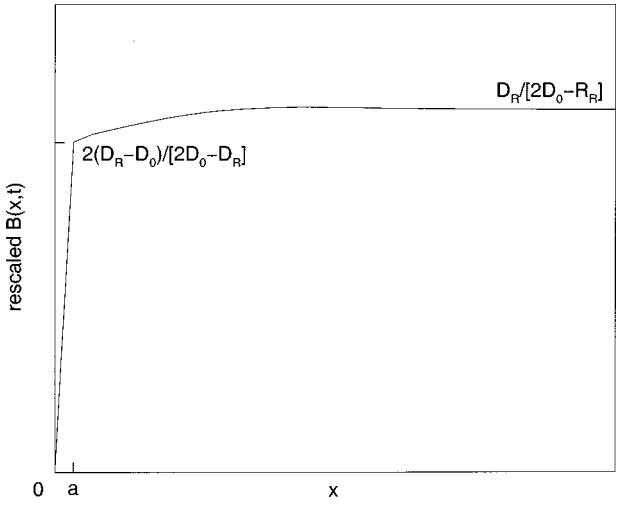

FIG. 3. Correlation function for the case of a random overload. B has been rescaled by the factor $A_0^2/[8\pi D_R t]^{1/2}$.

$$B(x=0,t) = 0,$$

$$B(x \gg a,t) = \frac{A_0^2}{\sqrt{8\pi D_R T}} \left[1 - e^{-x^2/8D_R t} + \frac{\sigma^2}{2[D_0 - D_R]} \times \left(\frac{1}{a} + \frac{x}{8D_R t} e^{-x^2/8D_R t} \right) \right], \tag{21}$$

which is shown in Fig. 3.

(b) Constant overload. In the same limit, we get $\tilde{C}(E) \sim 1/E$ or $\tilde{C}(t) = b_0$, where

$$b_0 = B_0^2 \frac{D_R}{2\pi[2D_0 - D_R]}.$$

Hence

$$B(x=0,t) = 0,$$

$$B(x \gg a,t) = \frac{\sigma^2 B_0^2}{4\pi[2D_0 - D_R]} \left[\frac{1}{a} - \frac{1 - e^{-x^2/8D_R t}}{\sqrt{8\pi D_R t}} \right], \tag{22}$$

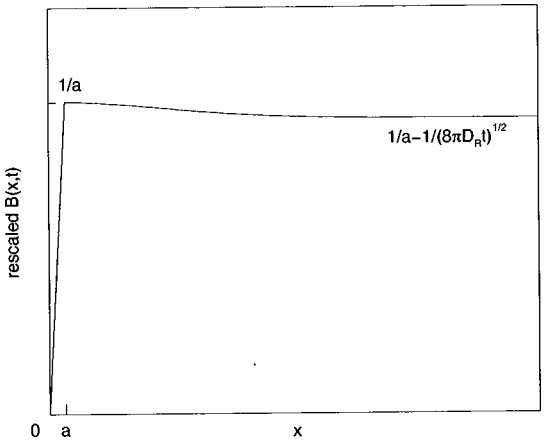

FIG. 4. Correlation function for the case of a uniform overload. B has been rescaled by the factor $\sigma^2 B_0^2/[4\pi(2D_0 - D_R)]$.

which has a form similar to that above; see Fig. 4.

One could have performed the calculation with the Ito convention (corresponding to the Liu *et al.* model). The final results for the correlation function are actually very similar to those above. The main point is that the correlation is rather structureless. Equation (22) shows that the correlation function $C(x>a,t)$ becomes zero for large times, a result that was used to establish Eq. (2).

3. Perturbation theory

The above method gives exact results, essentially because $v(x,t)$ is short-range correlated in time: $\delta\omega/\delta v$ is then only needed at coinciding times, where it is exactly known. This would not be true in general; furthermore, Novikov's theorem requires v to be Gaussian. It is thus interesting to show how a systematic perturbation scheme can be made to work by the use of diagrams to represent Eq. (9). The MCA is then a particular resummation scheme of this set of diagrams, which was discussed in detail in [18], which sometimes provide interesting nonperturbative results.

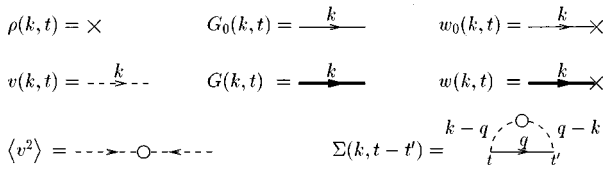

FIG. 5. Definition of various diagrams.

Equation (9) is multiplied on the left by the operator G_0 [see Eq. (10)] and then reexpressed as

$$w(k,t)=G_0(k,t)\otimes\rho(k,t)-ikG_0(k,t)\otimes\int\frac{dq}{2\pi}\,w(q,t)v(k-q,t), \tag{23}$$

$\otimes$ meaning a t-convolution product. This equation can be represented with diagrams as follows: As shown in Fig. 5, we represent the source ρ by a cross, the bare propagator G_0 by a plain line, and the noise v by a dashed line. The first term of Eq. (23), which is the noiseless solution w_0, is then obtained as the juxtaposition of a plain line and a cross. The arrow flows against time (i.e., it is directed from t to $t'<t$). The juxtaposition of two objects means a t-convolution product. By definition w is represented by the juxtaposition of a bold line and a cross (this is consistent with the identification of a bold line with the full propagator G). The diagrammatic version of Eq. (23) is then

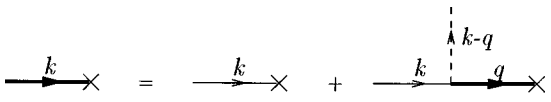

(24)

The ''vertex'' stands for $-ik\int(dq/2\pi)$, the two emerging wave vectors being q and $k-q$ (node law). One can now iterate this equation. To second order, one obtains

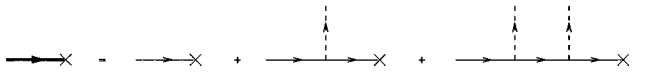

(25)

The corresponding equation for G is obtained by taking the derivative $\delta/\delta\rho$ and averaging over the noise v. Since $\langle v\rangle=0$, the second diagram vanishes. We represent the noise correlator by a dashed line with a centered circle (see Fig. 5) and obtain

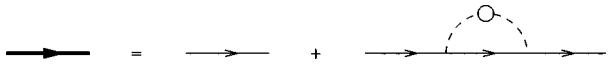

(26)

or $G=G_0+G_0\Sigma G_0$, where Σ is called the self-energy (see Fig. 5). Actually, one can resum exactly all the diagrams corresponding to $G_0\Sigma G_0$ and $G_0\Sigma G_0\Sigma G_0$ to obtain the Dyson equation $G=G_0+G_0\Sigma G$.

The MCA amounts to replacing the bare propagator in the diagram for Σ by the full propagator G. (Note that the MCA is of course exact to second order in perturbation theory). We then obtain a self-consistent equation for G:

$$\Sigma_{\mathrm{MCA}}=G_0^{-1}-G_{\mathrm{MCA}}^{-1}=$$

(27)

Diagrams like the one drawn in Fig. 6 are now also included.

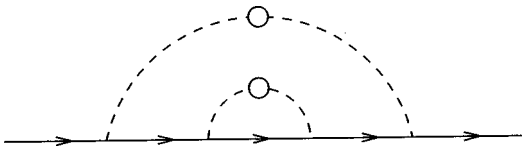

FIG. 6. Example of a diagram included in the MCA.

The self-energy Σ_{MCA} can be easily computed; we get

$$\Sigma_{\mathrm{MCA}}(k,t-t')=\sigma^2k\int\frac{dq}{2\pi}\,qG_{\mathrm{MCA}}(q,t-t')\times g_t(t-t'). \tag{28}$$

In the special case where g_t is peaked around $t=t'$, we can make the approximation $G(q,t-t')g_t(t-t')\simeq G(q,0)g_t(t-t')=g_t(t-t')$ [since by definition $G(q,0)=1$]. We thus get, using Eq. (8), $\Sigma_{\mathrm{MCA}}(k,t-t')=-\sigma^2\Lambda k^2g_t(t-t')/(2\pi)$. The expression for G_{MCA}^{-1} is thus identical to the one obtained with the exact approach, as can be seen by comparing Eq. (17) and $G_0^{-1}G=1+\Sigma G$.

Note that one can also calculate the influence of a nonzero kurtosis κ of the noise v, which is its normalized fourth cumulant. In this case, four dashed lines (corresponding to v) can be merged, leading to a contribution to D, of the order of $\kappa\sigma^4$.

Let us turn now to the calculation of the correlation function $\langle w(k,t)w(k',t)\rangle\equiv 2\pi\delta(k+k')C(k,t)$. The basic object

that corresponds to the self-energy is now the ''renormalized source'' spectrum $S(k,t,t')$ defined as $C=G\otimes S\otimes G$. The quantity S is drawn as a filled square. S_0 (empty square) is the correlation function source term, which encodes the initial conditions (see below). The two first terms of the expansion are

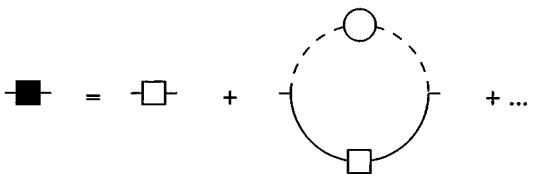

(29)

Here again we transform the perturbative expansion into a closed self-consistent equation for S by replacing G_0 and S_0 in Eq. (29) by G and S, respectively. The final equation for C reads

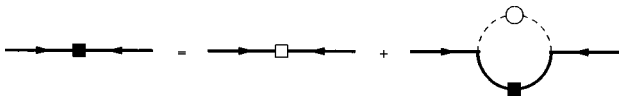

(30)

or, written explicitly,

$$C(k,t)=\int_0^t dt'\int_0^t dt''G(k,t-t')S_0(k,t',t'')G(-k,t-t'')$$
$$+\sigma^2k^2\int_0^t dt'\int_0^t dt''G(k,t-t')$$
$$\times\int\frac{dq}{2\pi}C(q,t',t'')g_t(t'-t'')G(-k,t-t''). \tag{31}$$

If we choose the source term to be an overload localized at $t=0$, we get $S_0=\langle\rho(k,t')\rho(-k,t'')\rangle=C(k,0)\delta(t')\delta(t'')$. Using the fact that g_t is peaked around $t'=t''$, we again recover exactly Eq. (19), showing again that the MCA is exact (in the limit $k\to 0$) in this special case.

D. Further results: The unaveraged response function

The *average* Green's function described above is thus a Gaussian of zero mean and of width growing as $\sqrt{D_R t}$. However, for a *given* environment, the Green's function is not Gaussian, presenting sample-dependent peaks (see Fig. 7). Note, however that, contrarily to what we shall find below for the tensorial case, the unaveraged Green's function remains everywhere positive. Furthermore, the quantity $[x](t)$, defined as the displacement of the centroid of the weight distribution beneath a point source in a given realization,

$$[x](t)=\int_{-\infty}^{+\infty}dx'x'\,\frac{\delta w(x',t)}{\delta\rho(0,0)}, \tag{32}$$

typically grows with t. More precisely, one can show that

$$\langle[x](t)\rangle=0 \quad \text{but} \quad \langle[x]^2(t)\rangle\propto t^{1/2}, \tag{33}$$

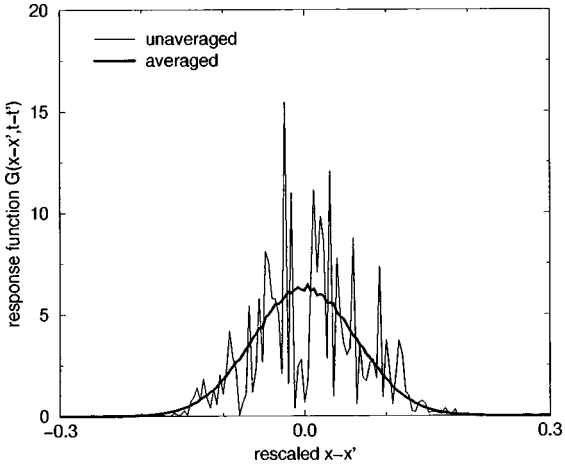

FIG. 7. Averaged (bold line) and unaveraged (thin line) response functions of the scalar model, obtained numerically by simulating the Liu *et al.* model. The average is performed over 5000 samples. One can notice how ''non-self-averaging'' the response function is, i.e., how different it is for a given environment as compared to the average. Note also that the unaveraged Green's function is everywhere positive.

meaning that the ''center'' of Green's function wanders away from the origin in a subdiffusive fashion, as $t^{1/4}$. This behavior has actually been obtained in an another context, that of a quantum particle interacting with a time-dependent random environment. Physically, the Liu *et al.* model can indeed be seen as a collection of time-dependent scatterers, converting incoming waves into outgoing waves with a certain partition factor $q_+=1-q_-$ (see the discussion in [19]). In two dimensions (plus time), the wandering of the packet center $[x](t)$ is only logarithmic (and disappears in higher dimensions [19]).

E. The scalar model with bias: Edwards's picture of arches

Up to now, we have considered the mean value of v to be zero, which reflects the fact that there is no preferred direction for stress propagation. In some cases, however, this may not be true. Consider, for example, a sandpile built from a point source: The history of the grains will certainly inprint a certain oriented ''texture'' to the contact network, which can be modeled, within the present scalar model, as a nonzero value of $\langle v\rangle$, the sign of which depends on which side of the pile is chosen. Let us call V_0 the average value of v on the $x\geqslant 0$ side of the pile and $-V_0$ on the other side. The differential equation describing propagation now reads, in the absence of disorder,

$$\partial_t w+\partial_x[V_0\,\mathrm{sgn}(x)w]=\rho+D_0\partial_{xx}w. \tag{34}$$

(An extra noise can be handled as above.) For a constant density $\rho=\rho_0$ and for $D_0=0$, the weight distribution is then

$$w(x,t)=\frac{\rho_0 x}{V_0} \quad \text{for } 0\leqslant x\leqslant V_0 t,$$
$$w(x,t)=\frac{\rho_0(ct-x)}{c-V_0} \quad \text{for } V_0 t\leqslant x\leqslant ct, \tag{35}$$

where $c=1/\tan(\phi)$ (ϕ is the angle made by the slope of the pile with the horizontal x axis). For $D_0 \neq 0$, the above solution is smoothed (see Fig. 8). In any case, the local weight reaches a *minimum* around $x=0$. Equation (34) gives a precise mathematical content to Edwards' model of arching in sandpiles [20], as the physical mechanism leading to a dip in the pressure distribution [21]. As discussed elsewhere [11,12], this can be taken much further within a tensorial framework (see Sec. III).

The scaling of the stress at the center of the pile $w(0,t)$ can be understood simply in terms of random walks subject to a bias V_0. The region contributing to $w(0,t)$ is then found to be of finite volume, independent of t, and of the order of D_0/V_0^2, as shown on the two top pictures of Fig. 8.

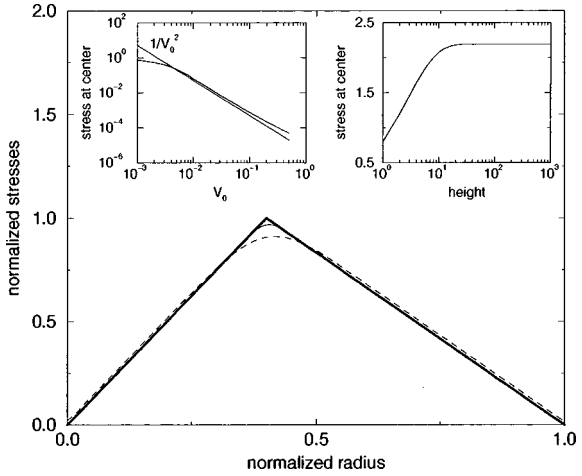

FIG. 8. On the main graph the solution of Eq. (34) for $V_0/c=0.4$ is plotted. The dashed line is for a diffusion constant D_0 ten times smaller than the solid one. The bold line is for $D_0=0$. Stress values are rescaled by the height of the pile t. The left inset shows that $w(0,t)$ scales like $1/V_0^2$ at small V_0, while the right inset shows that $w(0,t)$ is constant for large t. Note that for very small values of V_0, the $1/V_0^2$ scaling becomes invalid for finite-size reasons.

Equation (34) with noise can in fact be obtained naturally within an extended Liu *et al.* model, with an extra rule accounting for the fact that a grain can slide and lose contact with one of its two downward neighbors [3]. This generically leads to arching; in the sandpile geometry and for above a certain probability of (local) sliding, the effective velocity V_0 becomes nonzero and the weight profile (35) is recovered [3]. However, this extra sliding rule implicitly refers to the existence of shear stresses, which are absent in the scalar model but are crucial to obtain symmetry-breaking effects modeled by a nonzero V_0. It is thus important to consider from the start the fact that stress has a tensorial, rather than scalar, nature. This is what we investigate in the following section.

III. THE TENSORIAL MODEL

A. The wave equation

It is useful to start with a simple ''toy'' model for stress propagation, which is the analog of the model presented in Fig. 1. We now consider the case of three downward neighbors (see Fig. 9), for a reason that will become clear below. Each grain transmits to its downward neighbors not one, but two force components: one along the vertical axis t and one along x, which we call, respectively, $F_t(i,j)$ and $F_x(i,j)$. (We will restrict attention, in the following to two-dimensional piles, leaving extensions to three dimensions for further investigations.) For simplicity, we assume that the ''legs'' emerging from a given grain can only transport the vector component of the force parallel to itself (but more general rules could be invented). Assuming that the transmission rules are locally symmetric and that a fraction $p \leqslant 1$ of the vertical component travels through the middle leg, we find

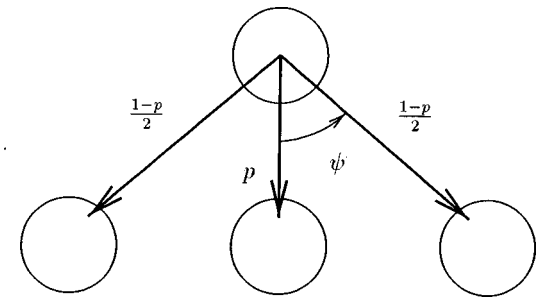

FIG. 9. Three-neighbor configuration. Each grain transmits two force components to its downward neighbors. A fraction p of the vertical component is transmitted through the middle leg and a fraction $(1-p)/2$ through each of the external legs.

$$F_x(i,j)=\tfrac{1}{2}[F_x(i-1,j-1)+F_x(i+1,j-1)] + \tfrac{1}{2}(1-p)\tan\psi[F_t(i-1,j-1)-F_t(i+1,j-1)], \tag{36}$$

$$F_t(i,j)=w_0+pF_t(i,j-1) + \tfrac{1}{2}(1-p)[F_t(i-1,j-1)+F_t(i+1,j-1)] + \frac{1}{2\tan\psi}[F_x(i-1,j-1)-F_x(i+1,j-1)], \tag{37}$$

where ψ is the angle between grains, defined in Fig. 9. Taking the continuum limit of the above equations leads to

$$\partial_t F_t+\partial_x F_x=\rho, \tag{38}$$

$$\partial_t F_x+\partial_x[c_0^2 F_t]=0, \tag{39}$$

where $c_0^2 \equiv (1-p)\tan^2\psi$. Eliminating (say) F_x between the above two equations leads to a *wave equation* for F_t, where the vertical coordinate t plays the role of time and c_0 is the equivalent of the ''speed of light.'' In particular, the stress does not propagate vertically, as it does in the scalar model, but rather at a *nonzero angle* φ such that $c_0=\tan\varphi$. Note that $\varphi \neq \psi$ in general (unless $p=0$); the angle at which stress propagates has nothing to do with the underlying lattice structure and can in principle be arbitrary. We chose a three-leg model to illustrate this particular point.

The above derivation can be reformulated in terms of classical continuum mechanics as follows. Considering all stress tensor components σ_{ij}, the equilibrium equation reads

$$\partial_t \sigma_{tt} + \partial_x \sigma_{xt} = \rho, \tag{40}$$

$$\partial_t \sigma_{tx} + \partial_x \sigma_{xx} = 0. \tag{41}$$

Identifying the local average of F_t with σ_{tt} and that of F_x with σ_{tx}, we see that Eqs. (38) and (39) are actually identical to Eqs. (40) and (41) provided $\sigma_{tx} = \sigma_{xt}$ (which corresponds to the absence of local torque) and $\sigma_{xx} = c_0^2 \sigma_{tt}$. This relation between normal stresses was postulated in [10] as the simplest constitutive relation obeying the correct symmetries that enables one to lift the indeterminacy of Eqs. (40) and (41); it can be seen as a *local* Janssen approximation [22]. c_0^2 should encode the relevant information of the local geometry of the packing, friction, shape of grains, etc., and should thus depend on the construction history of the grain assembly. For example, in the sandpile geometry c_0^2 is related to the angle of friction ϕ of the material by the relation $c_0^2 = 1/(1 + 2\tan^2 \phi)$ [10]. This approach can be generalized to take into account a local asymmetry in the packing texture (which one expects, for example, in the case of a sandpile constructed from a point source) by allowing c_0^2 to depend on σ_{xt}/σ_{tt} [10–12]. If this dependence is linear, this is equivalent to a coordinate rotation in x,t [12].

B. A stochastic wave equation

The starting point of the scalar model is thus essentially the diffusion equation, which one perturbs by adding a random convective term. As the preceding subsection shows, a more natural starting point is the wave equation. The toy model presented above, however, suggests that, provided local conservation laws are obeyed (i.e., those arising from mechanical equilibrium), many local rules for force transmission are compatible with the contact conditions [14]. It is thus natural to encode the disorder of the packing or model the indeterminacy of the contact conditions as a randomly varying speed of light c_0 (reflecting the fact that, for example, the parameter p can vary from grain to grain). Two recent numerical simulations [14,23] actually suggest that this should be a good first approximation. In Fig. 10 we show

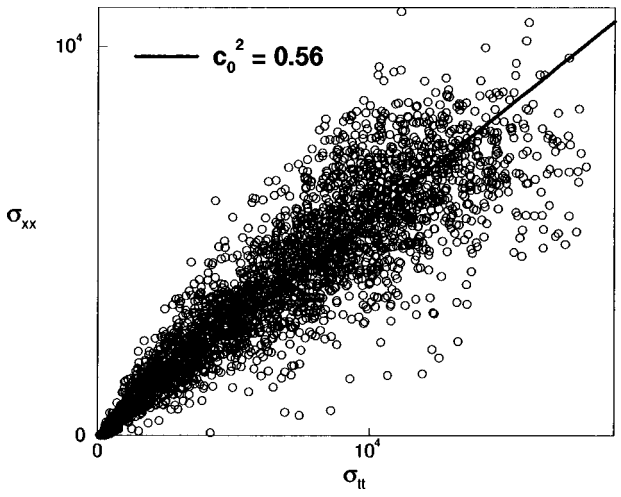

FIG. 10. Relation between σ_{xx} and σ_{tt} from a microscopic numerical simulation of grains forming a heap in two dimensions [23]. These data are compatible with a stochastic constitutive relation $\sigma_{xx} = c_0^2[1 + v(x,t)]\sigma_{tt}$, where v is the random noise.

a scatter plot of σ_{xx} versus σ_{tt}, measured as averages of the local forces over a small box centered around different points within a heap (from Ref. [23]). This plot clearly shows that a linear relation is indeed acceptable, leading in this case to $c_0^2 \sim 0.56 \pm 0.03$ [23]. There are, however, significant fluctuations, reflecting some disorder in the packing, which are furthermore uncorrelated from point to point. The histogram of v defined as

$$\sigma_{xx} = c_0^2[1 + v(x,t)]\sigma_{tt}, \quad \langle v(x,t) \rangle = 0, \tag{42}$$

is found to be roughly Gaussian, of relative width $\sigma \sim 0.3$. This corresponds to a locally varying angle of stress propagation, which varies around the mean angle 54° by an amount $\sim 10.8°$.

Motivated by the simulations results, we now investigate a model (called the random symmetric model in the following) with the inhomogeneous constitutive relation (42), which leads to the following stochastic wave equation for stress propagation:

$$\partial_{tt} \sigma_{tt} = \partial_{xx} \{ c_0^2[1 + v(x,t)]\sigma_{tt} \}, \tag{43}$$

where the random noise v is assumed to be correlated as $\langle v(x,t)v(x',t') \rangle = \sigma^2 g_x(x - x') g_t(t - t')$. The correlation lengths ℓ_x and ℓ_t are again kept finite and of the same order of magnitude. In a Fourier transform, this relation can also be written $\langle v(k,t)v(k',t') \rangle = 2\pi\sigma^2 \delta(k + k') \tilde{g}_x(k) g_t(t - t')$. It turns out that the final shape of the averaged response function depends on the sign of $\tilde{g}_x(\Lambda)$. In Sec. II we implicitly made the choice $\tilde{g}_x(k) = 1$, which corresponds to $g_x(x = 0) = 1/a$ and $g_x(x > 0) = 0$. We will keep this choice for the following calculations, but note that another form for g_x could lead to $\mathrm{sgn}[\tilde{g}_x(\Lambda)] = -1$.

In the following, σ_{tt} will be again denoted by w. After a Fourier transform along the x axis, we get, from Eq. (43),

$$(\partial_{tt} + c_0^2 k^2) w = \partial_t \rho - c_0^2 k^2 \int \frac{dq}{2\pi} w(q,t) v(k - q, t). \tag{44}$$

Note that the ''source'' term of this equation is now $\partial_t \rho$ rather than ρ itself. Therefore, if we call G the Green's function (or propagator) of this equation $G = \langle \delta w / \delta \partial_t \rho \rangle$; the response function $R = \langle \delta w / \delta \rho \rangle$ of our system is now actually the time derivative of G: $R(k,t) = \partial_t G(k,t)$.

The noiseless propagator G_0 is the solution of the ordinary wave equation $(\partial_{tt} + c_0^2 k^2) G_0(k, t - t') = \delta(t - t')$ and can be easily calculated:

$$G_0(k,t) = \frac{1}{2ic_0 k} [e^{ic_0 kt} - e^{-ic_0 kt}] \theta(t), \tag{45}$$

which leads to the response function R_0,

$$R_0(x,t) = \tfrac{1}{2}[\delta(x - c_0 t) + \delta(x + c_0 t)] \theta(t). \tag{46}$$

Equation (46) sums up one of the major results of [10] (see also [11–12]): In two dimensions, stress propagates along two characteristic rays. [Note that the corresponding response function in three dimensions (where a secondary closure is needed, for instance, $\sigma_{xx} = \sigma_{yy}$, y being the third

coordinate) reads $R_0(x,t) \propto (c_0^2 t^2 - x^2)^{-1/2}$ for $|x| < c_0 t$ and zero otherwise [10]]. A relevant question is now to ask how these rays survive in the presence of disorder. We will show that for weak disorder, the δ peaks acquire a finite (diffusive) width and that the speed of light is renormalized to a lower value. Not surprisingly, the effect of disorder can be described by an ''optical index'' $n>1$. For a strong disorder, however, we find (within a Gaussian approximation for the noise v) that the speed of light vanishes and then becomes imaginary. The ''propagative'' nature of the stress transmission disappears and the system behaves more like an elastic body, in a sense clarified below.

C. Calculation of the average response function

One can again use Novikov's theorem in the present case if the noise is Gaussian and short-range correlated in time. However, the same results are again obtained within the diagrammatic approach explained in Sec. II, which can be easily transposed to the present case, and is more general. The propagator G is a now represented as a line, the source $\partial_t \rho$ a cross and the vertex meaning $-c_0^2 k^2 \int (dq/2\pi)$. Within the MCA, the self-consistent equation [analogous to Eq. (27) in the scalar case] is

$$(\partial_{tt} + c_0^2 k^2) H(k,t) = \delta(t) + \int_0^t dt' \Sigma_{\mathrm{MCA}}(k,t') H(k,t-t'), \tag{47}$$

where H is defined by $G(k,t) = H(k,t)\theta(t)$ and the self-energy Σ_{MCA} is given as

$$\Sigma_{\mathrm{MCA}}(k,t-t') = c_0^4 \sigma^2 k^2 \int \frac{dq}{2\pi} q^2 g_t(t-t') \times \tilde{g}_x(k-q) H(q,t-t'). \tag{48}$$

Equation (47) can be solved using a standard Laplace transform along the t axis (E is the Laplace variable). Using the fact that $H(k,\tau) = \tau$ in the limit where $\tau \to 0$, we find, for small k,E (corresponding to scales L such that $\ell_x, \ell_t \ll L$), $H^{-1}(k,E) = E^2 + \beta E + c_R^2 k^2$, where

$$c_R^2(k) = c_0^2 - \frac{c_0^4 \sigma^2 \Lambda^3 \ell_t}{12\pi} \left(1 - \frac{3|k|}{2\Lambda}\right) + O(k^2), \tag{49}$$

$$\beta(k) = \frac{c_0^4 \sigma^2 k^2 \Lambda^3 \ell_t^2}{18\pi} + O(k^3). \tag{50}$$

We notice here that in the limit $\ell_t \to 0$, the effect of the randomness completely disappears, as in the scalar model with the Ito convention. [Technically, this is due to the fact that $G(k,t=0) \equiv 0$ in the present problem.] In order to calculate the inverse Laplace transform, we need to know the roots of the equation $H^{-1}(k,E) = 0$. This leads to several phases, depending on the strength of the disorder.

1. The weak-disorder limit

For weak disorder, $c_R^2(k)$ is always positive. We can then define $c_R = c_R(k=0)$. As we will show now, c_R is the shifted cone angle along which stress propagates asymptotically. c_R is a decreasing function of σ, meaning that the peaks of the response function get closer together as the disorder increases. [As a technical remark, let us note that if $g_t = g_x$, the problem is symmetric in the change $x \to t$, $c_0^2(x,t) \to 1/c_0^2(x,t)$. It thus looks as if the cone should both narrow or widen, depending on the arbitrary choice of x and t. There is, however, no contradiction with the above calculation since we assumed that v has zero mean, while $1/(1+v) - 1$ has a positive mean value, of order σ^2.] For a critical value $\sigma = \sigma_c$, c_R vanishes and becomes imaginary for stronger disorder. For $\ell_t = \ell_x = 1$ and $c_0^2 = 0.6$ (corresponding to $\phi = 30°$), one finds $\sigma_c \simeq 1.42$.

In the limit of large t, the propagator reads

$$G(k,t) = \frac{1}{c_R k} \sin[c_R k t (1 + \alpha |k|)] e^{-\gamma k^2 t} \theta(t), \tag{51}$$

where the following constants have been introduced [note that the sign of α is dictated by the sign of $\tilde{g}_x(\Lambda)$]:

$$\alpha = \frac{3}{4\Lambda} \left(\frac{c_0^2}{c_R^2} - 1 \right), \tag{52}$$

$$\gamma = \frac{\beta(k)}{2k^2} = \frac{\sigma^2 \Lambda^3 \ell_t^2}{36\pi}. \tag{53}$$

From Eq. (51) the response function R, in the limit of small k and large t, is given by

$$R(k,t) = \cos[c_R k t (1 + \alpha |k|)] e^{-\gamma k^2 t} \theta(t) \tag{54}$$

or in real space

$$R(x,t) = \frac{1}{2\sqrt{4\pi |\hat{\gamma}|(t)}} \mathrm{Re} \left\{ \frac{e^{-\xi_+^2/b}}{\sqrt{b}} \left[1 - \Phi\left(-i \frac{\xi_+}{\sqrt{b}} \right) \right] + \sqrt{b} e^{-b\xi_-^2} [1 - \Phi(-i\sqrt{b}\xi_-)] \right\}, \tag{55}$$

where the scaling variables $\xi_\pm$, measuring distances relative to the two peaks, are defined by

$$\xi_\pm = \frac{x \pm c_R t}{\sqrt{4|\hat{\gamma}| t}} \tag{56}$$

and where $\hat{\gamma} = \gamma - i c_R \alpha$ and $b = e^{i \arg \hat{\gamma}}$. Φ is the standard error function. Figure 11 shows R as given by expression (55). Interestingly, this propagator not only has a finite diffusive width proportional to $\sqrt{t}$, but is also asymmetric around its maxima. Surprisingly, and in sharp contrast to the scalar case discussed above, the response function becomes *negative* in certain intervals (although its integral is of course equal to one because of weight conservation). This means that pushing on a given point actually reduces the downward pressure on certain points. This can be interpreted as some kind of arching: Increasing the shear stress does affect the propagation of the vertical stress and may indeed lead to a reduction in its local value that is redistributed elsewhere. As we shall see in Sec. V, the unaveraged response function indeed takes negative (and rather large) values. This is a very

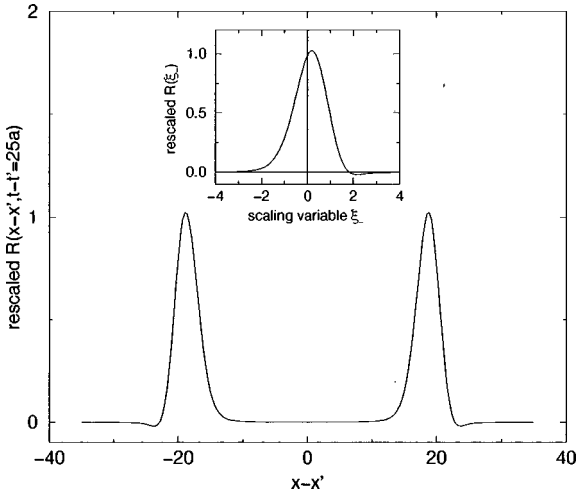

FIG. 11. Response function for weak disorder ($\sigma/\sigma_c \sim 0.13$). The two curves have been rescaled by the factor $2[4\pi|\tilde{\gamma}|t]^{1/2}$. The main graph shows the general double-peaked shape of the response of the system when subjected to a peaked overload at $x=0$, $t=0$. The inset gives details the right-hand peak as a function of the scaling variable ξ_-. Note the asymmetry [for $\tilde{g}_x(\Lambda)>0$], compatible with the results found in [14]. Note also that the curve becomes negative around $\xi_-=2$.

significant result since it suggests that granular materials may be susceptible to rearrangement under extremely weak external perturbations. Suppose indeed that as a result of the perturbation a grain receives a negative force larger than the preexisting vertical pressure. This grain will then move and a local rearrangement of contacts will occur, inducing a variation of $c_0(x,t)$ as to reduce the cause of the instability. Thus the stochastic wave equation implicitly demands rules similar to those introduced in [3] to describe extreme sensitivity to external perturbations in silos. The present model, which is purely static, does not say what to do when a local rearrangement occurs, but certainly suggests that small perturbations will induce such rearrangements.

It is interesting to note that this response function was numerically measured in Ref. [14]; its shape is compatible with the above expression; in particular, the two peaks were found to be asymmetric with a longer ''tail'' extending inward, as we obtain here. Note, however, that for $\tilde{g}_x(\Lambda)<0$, the shape of the peaks is reversed: The small dips are located inside the peaks and the longer tail extends outward. This is actually what we obtain numerically in Sec. V.

2. Shear response function

Equation (40) provides a straightforward way to calculate the shear response function R_s in terms of R. Indeed, one has $ikR_s(k,t)=\delta(t)-\partial_t R(k,t)$. We thus get, in the limit of small k and large t,

$$R_s(k,t)=-ic_R\sin[c_R kt(1+\alpha|k|)]e^{-\gamma k^2 t}\theta(t), \quad (57)$$

This shear response function is very similar to R, except that it is, as expected, an odd function of x.

3. Effective large-scale equations

It is interesting to know of which differential equations the response functions R and R_s are solutions. These effective equations can be interpreted as a coarse-grained (hydrodynamical) description of the propagation of a stress perturbation, which takes into account the average effect of the local disorder. One problem, however, comes from the presence of the dispersion term $\alpha|k|$, which corresponds to a nonlocal operator in real space. We thus neglect this term in the following discussion, but one should keep in mind that the effective equation are actually nonlocal. In any case, the main features of the response functions [peaks centered around $x=\pm c_R t$ ($c_R<c_0$) with a diffusive width proportional to $\sqrt{t}$] are not lost when setting $\alpha=0$ (except for the fact that the response function can become negative, which is related to $\alpha\neq 0$). Effective equations can then be written in the large-t limit as

$$\partial_t\langle\delta\sigma_{tt}\rangle=\delta\rho-\partial_x\langle\delta\sigma_{xt}\rangle, \quad (58)$$

$$\partial_t\langle\delta\sigma_{xt}\rangle=-c_R^2\partial_x\langle\delta\sigma_{tt}\rangle+2\gamma\partial_{xx}\langle\delta\sigma_{xt}\rangle. \quad (59)$$

That disorder generates the diffusion terms $2\gamma\partial_{xx}\langle\delta\sigma_{xt}\rangle$ is rather intuitive and had been guessed in [10]. This term can be seen as the first term of a gradient expansion of the constitutive equations, which have the correct symmetry, i.e.,

$$\langle\delta\sigma_{xx}\rangle=c_R^2\langle\delta\sigma_{tt}\rangle-\gamma\partial_x\langle\delta\sigma_{xt}\rangle, \quad (60)$$

$$\langle\delta\sigma_{tx}\rangle=\langle\delta\sigma_{xt}\rangle. \quad (61)$$

Equation (61) is imposed by the absence of local torque.

We have thus shown that the introduction of a small disorder in the local direction of propagation does not change radically the nature of stress propagation on large length scales, although the peaks in the response function acquire a diffusive width. These peaks acquire a width of the order of $\sqrt{\gamma H}$ (where H is the height of the pile) and are thus well separated in the limit where $H\gg\gamma$. As we shall see now, this is no longer true if the disorder becomes strong.

4. Critical disorder: The wave-diffusion transition

When the disorder is so strong that c_R just vanishes, the roots of $H^{-1}(k,E)=0$ change nature and so does the response function R. The two peaks of the previous expression for R merge together, while the width becomes anomalously large (proportional to $t^{2/3}$). In the asymptotic, large-t regime we obtain

$$R(k,t)=\theta(t)\cos[\lambda|k|^{3/2}t]e^{-\gamma k^2 t}, \quad (62)$$

where the new constant λ is defined by $\lambda=c_0\sqrt{3/2\Lambda}$ and $\gamma=c_0^2\ell_t/3$. The physical response function R is plotted in Fig. 12, for different values of t, as a function of the scaling variable

$$\xi=\frac{x}{\lambda t^{2/3}}. \quad (63)$$

On the scale $t^{2/3}$, the double-peak structure of R is still visible. However, note that the term $e^{-\gamma k^2 t}$ cannot be neglected, even for large t; this means that the response function is

never really a function of ξ only, as is clear from Fig. 12. Note that the response function again becomes negative for some values of ξ.

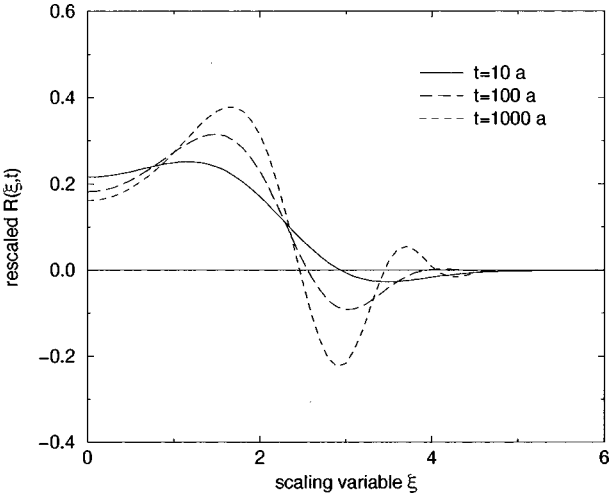

FIG. 12. Response function for a critical disorder $c_R=0$.

5. Strong disorder: The pseudoelastic regime

For larger disorder still, one finds, within the MCA (which is exact for a Gaussian, uncorrelated noise), that the renormalized value of c_0^2, c_R^2 becomes negative. Upon a rescaling of x as $\hat{x}=x/ic_R$, the effective equation on $\langle \delta\sigma_{tt}\rangle$ then becomes, on large length scales, Poisson's equation

$$\nabla^2\langle \delta\sigma_{tt}\rangle=\partial_t\langle \delta\rho\rangle, \tag{64}$$

which means that the stress propagation becomes somewhat similar to that in an elastic body, where stresses obey an elliptic equation of similar type [24]. In particular, the cone structure of stress propagation, which is associated with the underlying, hyperbolic, wave equation finally disappears; the average response to a localized perturbation becomes a broad ''bump'' of width comparable to the height of the pile. It is thus rather interesting to see that, within the MCA, there is a phase transition from a wavelike mode to a diffusive mode of stress propagation; the observation of the cone thus requires that the packing is not too disordered. Certainly for relatively ordered packings the cone exists and has been observed experimentally [25] and numerically [14,23]. One should, however, add some remarks.

(i) It is possible that the above transition is an artifact, due to the fact that v is taken to be Gaussian, which, strictly speaking, is not allowed since the local value of c_0^2 should always be positive. One can show for some other problems of the same type that a similar transition is artificially induced by the Gaussian approximation when it cannot really exist on physical grounds. In this respect, it is interesting to note that the first non-Gaussian correction tends to increase c_R for negative kurtosis, as might be expected for a bounded v distribution.

(ii) It should be noted that the predicted effective constitutive relation between horizontal and vertical normal stresses has a negative sign if $c_R^2<0$. This means that increasing the vertical stress should reduce the horizontal stress, which is only possible if the grains move. Hence the region where $c_R^2<0$ is probably impossible to reach physically: The system will rearrange spontaneously to reduce the disorder and to make $c_R^2\geqslant 0$. As already discussed above, the disorder that results from such a rearrangement might be strongly correlated and correspond to an arching effect, as in [3].

D. The correlation function

Returning to the weak-disorder case, the major problem for the direct observation of the light cone is the fact that the perturbation representing the point source should be small (otherwise the packing structure would changes in an inhomogeneous way, thereby affecting the value of c_0^2 in a nonuniform way), but large enough for the response to be detected. A better possibility, as we show now, could be to measure the correlation function of the stress field. We again consider the stress correlation function in the case where the mass of each grain is small ($\rho=0$) and a random or a constant overload is applied on the top of the silo. With the new convention for the bar (for G) and the cross (for $\partial_t\rho$), the self-consistent diagrammatic equation (30) is valid in the tensorial case. When writing it in its usual mathematical form, the only difference from the scalar model is that now the weight source term is $w(k,0)\delta'(t)$, leading to $S_0(k,t',t'')=C(k,0)\delta'(t')\delta'(t'')$.

The calculation of the correlation function is very similar to the scalar case. In order to carry out the calculations to the end, we have neglected the dispersion term $\alpha|k|$ in the expressions for G and R. The analog of Eq. (20) is now, for weak disorder,

$$C(k,t)=C(k,0)\cos^2[c_Rkt]e^{-2\gamma k^2}+\sigma^2\frac{c_0^4}{c_R^2}k^2\int_0^t dt'\sin^2[c_Rk(t-t')]e^{-2\gamma k^2(t-t')}C(t'). \tag{65}$$

The function $\tilde{C}(t')=\int(dk/2\pi)C(k,t')$ is of identical form to the scalar case; only the expressions for a_0 (for the random overload) and b_0 (for the constant overload) are different:

$$a_0=\frac{A_0^2}{4\sqrt{2\pi\gamma}}\frac{1}{1-\dfrac{\sigma^2c_0^4}{4\pi\gamma^2c_R^2}\arctan\left(\dfrac{\pi\gamma}{c_R}\right)}, \tag{66}$$

$$b_0=\frac{B_0^2}{2\pi}\frac{1}{1-\dfrac{\sigma^2c_0^4}{4\pi\gamma^2c_R^2}\arctan\left(\dfrac{\pi\gamma}{c_R}\right)}. \tag{67}$$

Knowing $\tilde{C}(t')$, $C(x,t)$ can be computed from Eq. (65). For the case of a constant overload, the shape of the correlation function is very close to the one shown in Fig. 4 for the scalar model. The case of the random overload, however, is much more interesting since the fact that information travels along a cone of angle c_R appears clearly: The correlation function presents *two* peaks. The first one is of course at $x=0$, while the second is at $x=2c_Rt$, which simply means

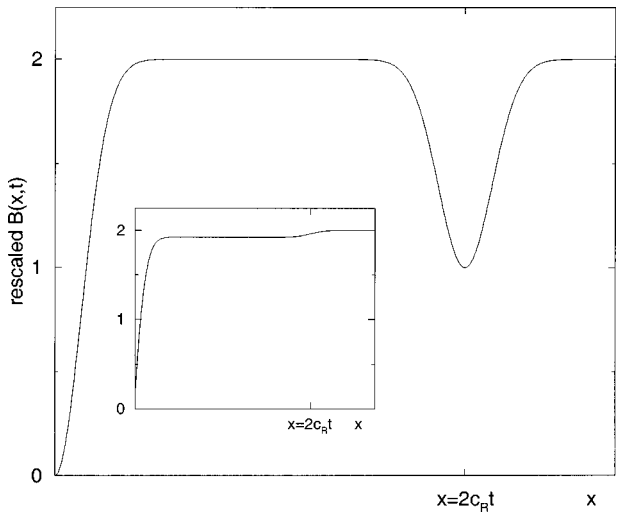

FIG. 13. Correlation function for the case of a random overload. Note the presence of a peak centered at $x=2c_Rt$, which reflects the fact that information in the tensorial model is traveling along a cone of angle of c_R. In the case of a fluctuating density in the bulk of the pile, one should integrate Eq. (68) with respect to t. The result is plotted in the inset: The correlation reaches rapidly a first plateau and then increases again to a higher value around $x=2c_Rt$. The relative difference of height between the two plateaus decreases as $t^{-1/2}$.

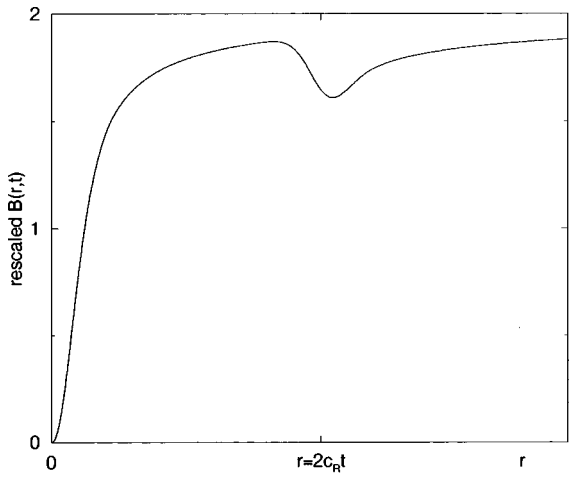

FIG. 14. Correlation function for three-dimensional disordered packings with a random overload, neglecting again the second term in Eq. (65). Note that, as in two dimensions, the correlation function exhibits a peak around $r=2c_Rt$.

that the two points at the bottom of the information cone share the same information coming from the apex of this cone. (In the absence of disorder, the correlation function consists of two δ peaks, one at $x=0$ and the other at $x=2c_0t$ of half the amplitude.) If we forget the second term of the right-hand side of Eq. (65), which is negligible compared to the first one at large t, we can see that the second peak of the correlation function has a width proportional to $\sqrt{t}$ and a height proportional to $1/\sqrt{t}$. This approximation is actually equivalent to saying that the (linear) effective equations (58) and (59) are sufficient to calculate the correlation function for large times. Other source terms, such as a fluctuating density in the bulk of the pile, can thus be easily accommodated by linear superposition. We have thus plotted in Fig. 13 the quantity $B(x,t)=C(0,t)-C(x,t)$, omitting the second term on the right-hand side of Eq. (65). Analytically, we have

$$B(x,t)=\frac{A_0^2}{4\sqrt{8\pi\gamma t}}\,[2+2e^{-c_R^2t/2\gamma}-2e^{-x^2/8\gamma t} -e^{-(x+2c_Rt)^2/8\gamma t}-e^{-(x-2c_Rt)^2/8\gamma t}]. \qquad (68)$$

This result is of importance since the shape of this correlation function clearly differs from the corresponding one in the scalar model. Measuring carefully the averaged correlation function of a granular system could then confirm (or disprove) the presence of a light raylike propagation. In this respect, it is interesting to plot the correlation function for three-dimensional packings as well. This correlation function only depends on the radial distance r between the two points, as is plotted in Fig. 14. We note that, much as in two dimensions, the correlation decreases sharply on the scale of a few grains, but increases again for distances of the order of the height of the pile. Note that a stress correlation function was actually measured recently in [6] and found to be featureless, but on very short scales $x\leqslant 5a$, as compared to the height of the pile $H\simeq 100a$. We expect the features of the correlation function to show up on much larger scales $\sim 2c_RH$.

IV. GENERALIZED WAVE EQUATIONS

It is tempting to generalize Eqs. (38) and (39) and write the most general linear equations governing the propagation of the forces that are compatible with the (local) conservation rules. These equations were originally written by de Gennes [26]:

$$\partial_tF_t+\partial_x[\,\eta'(x,t)F_x+\mu'(x,t)F_t]=\rho, \qquad (69)$$

$$\partial_tF_x+\partial_x[\,\eta(x,t)F_t+\mu(x,t)F_x]=0. \qquad (70)$$

Note that the terms μ,μ' break the symmetry $x\rightarrow -x$. This is allowed locally and does not show up on large scales if their average is zero. Another possibility (but without noise), considered in detail in [12], is that $\mu(x,t)$ changes sign with x, i.e., $\mu(x,t)=\mu\ \mathrm{sgn}(x)$, which describes the fact that the texture of a sandpile depends on which ''side'' of the pile one is looking at. Interestingly, Eqs. (69) and (70) still lead to wavelike propagation, but now the bisector of the light cone makes a nonzero angle with the vertical (when μ or μ' are nonzero). In other words, Eqs. (69) and (70) describe a situation where not only the opening angle of the cone can vary in space, but also its average orientation.

The same analytical techniques as above can be still be used. We shall only discuss some special cases. (To lowest order in perturbation theory, the case where disorder in present in the four terms η,η',μ,μ' simultaneously is very simply obtained by adding the corrections induced by each term taken individually.)

(i) Let us first set $\mu=\mu'=0$ and consider the case where η' is random and η fixed (and equal to c_0^2). Taking $\eta'(x,t)=\eta_0'[1+v(x,t)]$ with the noise v as above, one finds that the renormalized value of η' is

$$\eta_R' = \eta_0' \left(1 - \frac{c_0^2 \eta_0' \sigma^2 \Lambda^3 l_t}{12\pi} \right). \tag{71}$$

Now, on large length scales, one must recover the continuum equilibrium equations for the stress tensor [Eqs. (40) and (41)]. The condition of zero torque requires that the stress tensor is symmetric and thus one must set $\eta_R' \equiv 1$, which imposes a relation between η_0' and the amplitude of the noise σ. Note that beyond a certain value of σ, this relation can no longer be satisfied with a real η_0'. This again means that the packing is unstable mechanically and will rearrange so as to reduce the disorder.

(ii) Another interesting class of models, which one can call μ models, is such that $\eta = c_0^2$ and $\eta' = 1$, but $\mu(x,t) = c_0 v(x,t)$ and $\mu' = 0$ or vice versa. These two cases yield identical results, namely, in the large-t limit

$$R(k,t) = \cos(c_0 k t) e^{-\gamma k^2 t} \theta(t), \tag{72}$$

$$R_s(k,t) = -ic_0 \sin(c_0 k t) e^{-\gamma k^2 t} \theta(t), \tag{73}$$

where $\gamma = c_0^2 \Lambda \sigma^2/(8\pi)$. Note that in these cases, the response peaks acquire a finite diffusive width proportional to $\sqrt{t}$, but the angle of the information cone is unaffected by the disorder (i.e., c_0 is not renormalized).

(iii) Finally, there are special ''symmetry'' conditions where the equations can be decoupled and reduced to two scalar models. We will refer to this case as the ''double scalar'' model. This occurs when $\mu = \mu' = c_0 v_1(x,t)$ and $\eta' = \eta/c_0^2 = 1 + v_2(x,t)$ where v_1, v_2 are two different sets of noise. Let us define $\sigma_\pm = c_0 F_t \pm F_x$, $x_\pm = x \mp c_0 t$, and $v_\pm = v_1 \pm v_2$; we then obtain

$$\partial_t \sigma_+ = c_0 \rho - c_0 \partial_{x_+} [v_+ \sigma_+], \tag{74}$$

$$\partial_t \sigma_- = c_0 \rho - c_0 \partial_{x_-} [v_- \sigma_-], \tag{75}$$

showing that σ_+ and σ_- decouple, each propagating along two rays, of velocity $\pm c_0$, plus a small noise $v_\pm$, which, as in the scalar case, generates a nonzero diffusion constant. The response functions for σ_{tt} and σ_{xt} are thus again made of two diffusive peaks of width proportional to $\sqrt{t}$, centered at $x = \pm c_0 t$. The interest of this double scalar limit is that one can deduce simply the probability distribution of the stresses from the Liu *et al.* model. This is developed below. Note also that, by construction, this special form of disorder does not lead to negative vertical stresses.

V. STRESS DISTRIBUTION WITHIN THE TENSORIAL MODEL

A physically relevant question is to know how local stresses are distributed. We have seen above that within a scalar approach, an exponential-like distribution (possibly of the type $\exp(-w^\beta)$, with $\beta \geqslant 1$) is expected [4,9]. One can wonder whether this exponential distribution survives within a tensorial description and what happens for very small stresses $w \to 0$. Unfortunately, the full distribution can only be computed analytically for the double scalar model; but numerical results have also been obtained for the random symmetric model and are described below.

A. The double scalar limit

In the double scalar limit, the histogram of the stress distribution is obtained trivially by noting that since $\sigma_+ = w_1$ and $\sigma_- = w_2$ travel along different paths, they are independent random variables. Taking c_0 to be unity for simplicity, one thus finds

$$P(\sigma_{tt}) = \int dw_1 \int dw_2 P^*(w_1) P^*(w_2) \delta\left(\sigma_{tt} - \frac{w_1 + w_2}{2} \right), \tag{76}$$

$$P(\sigma_{xt}) = \int dw_1 \int dw_2 P^*(w_1) P^*(w_2) \delta\left(\sigma_{xt} - \frac{w_1 - w_2}{2} \right), \tag{77}$$

where P^* is the distribution of weight pertaining to the scalar case, which, as mentioned above, depends on the specific form of the local disorder and on the discretization procedure. In the strong-disorder case that leads to Eq. (3) (in the case $N = 2$), we thus find that $P(\sigma_{tt})$ is still decaying exponentially (it is actually a Γ distribution of parameter $2N$), although its variance is reduced by a factor 2. For $N = 2$, one simply gets

$$P(\sigma_{tt}) = \tfrac{8}{3} \sigma_{tt}^3 e^{-2\sigma_{tt}}, \tag{78}$$

$$P(\sigma_{xt}) = (|\sigma_{xt}| + \tfrac{1}{2}) e^{-2|\sigma_{xt}|}. \tag{79}$$

The preexponential factor is therefore noticeably different from the prediction of Eq. (3).

B. Numerical histograms for the random symmetric model and open problems

The numerical analysis of Eqs. (40) and (41), with a stochastic constitutive relation $\sigma_{xx} = \eta[1 + v(x,t)]\sigma_{tt}$, is actually not an easy task and the final results depend rather sensitively on the chosen discretization. For example, a naive discretization of the random wave equation leads to a nonzero diffusive width even in the absence of disorder and thus makes it hard to measure the ''true'' response function, which should, in the absence of disorder, consist of two δ peaks. However, it should be noted that such diffusive term (or order a) are actually expected physically: They indeed appear when Eqs. (36) and (37) are expanded to second order in the lattice spacing. We shall return to this point below.

The method we chose is the following. Starting with points regularly arranged at $t = 0$, we construct the network of characteristics (in the mathematical sense). Associated with each point (x,t) is a speed of light $c_0(x,t) = c_0\sqrt{[1 + v(x,t)]}$, which determines the directions of lines that propagate the component of the stress parallel to that line, away from the point (x,t). The point (x,t) is then generated by two ''parents'' points (x',t') and (x'',t'') as indicated in Fig. 15(a). It sometimes happens that the cone from (x',t') is so wide that it cannot intersect with the one from (x'',t'') [see Fig. 15(b)]. We then impose $x = x''$ and $t = t''$. This actually can be viewed as a local kind of arching: The point (x'',t'') supports not only its parent neighbors but also its ''same generation'' neighbor (x',t'). This method has several advantages. Its physical interpretation is very clear: Points are ''grains'' and characteristics are ''stress paths.''

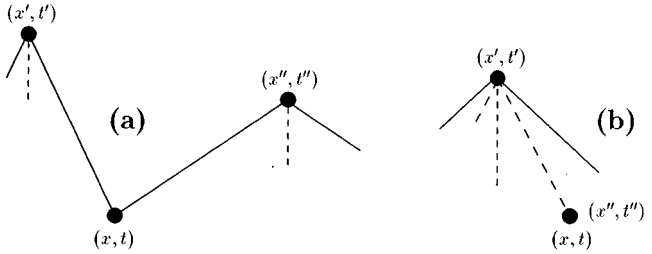

FIG. 15. The left-hand picture (a) shows the construction rule of the characteristics network: The ''child'' point (x,t) is located at the intersection of the cones from the two ''parent'' points (x',t') and (x'',t''). When the cones do not intersect (b), we choose (x,t) and (x'',t'') to be coincident.

Figure 16 shows an example of the network of those paths. We can see how stress paths actually merge together and generate arching. Furthermore, there is strictly no diffusion in the absence of disorder, i.e., the Green's function is exactly given by the sum of two δ peaks.

Although the noise v has been implicitly considered to be Gaussian throughout this paper, for numerical simplicity we chose the following algorithm for the calculation of $v(x,t)$. At each site (x,t), a random angle θ is uniformly chosen between $-\Delta(\pi/4)$ and $\Delta(\pi/4)$. Δ controls the amplitude of the noise. We then set $c_0(x,t)=c_0\tan[\pi/4+\theta(x,t)]$; v and θ are then related by $v(x,t)=4\tan\theta(x,t)/[1-\tan\theta(x,t)]^2$. However, since the lattice itself is generated by the disorder, the precise correlation function g_x of the v's is not well controlled in this numerical scheme. This is rather important since we showed in Sec. III that the structure of g_x influences the shape of the response function (it determines whether the negative part of the response lies on the inward or outside edge of the main peak). In fact, the structure of the peaks we obtain numerically is reversed compared to that of our analytical calculation; see Fig. 17.

The numerical histogram of the force distribution at the bottom of a silo computed within this numerical scheme immediately reveals some problems. Since the lattice becomes more distorted as time increases, the numerical histogram of vertical forces keeps broadening and never reaches a stationary shape. Furthermore, there is a nonzero probability of ob-

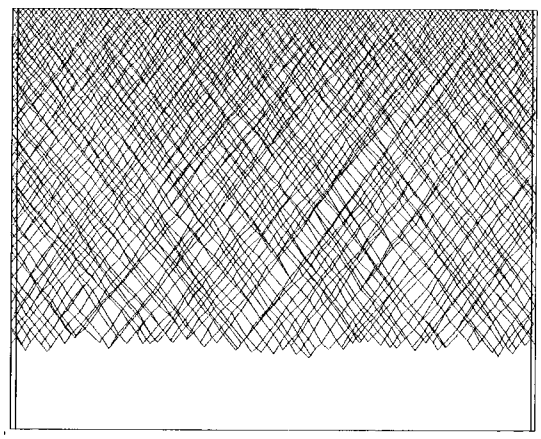

FIG. 16. Stress path network for a periodic silo of width $100a$. This picture has been computed with $\Delta=0.2$. We have chosen periodic lateral boundary conditions.

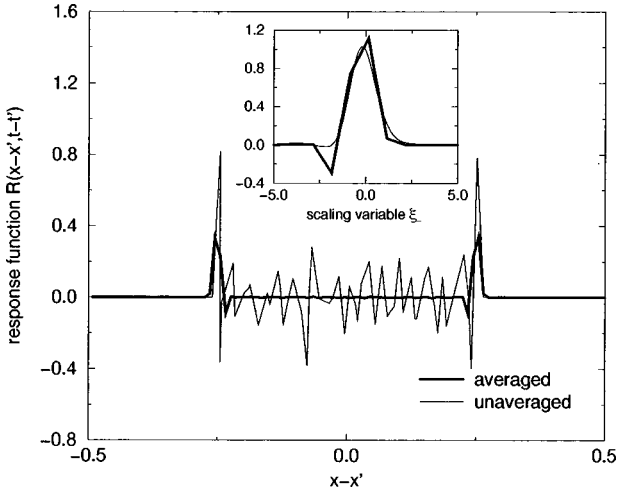

FIG. 17. The main graph shows the response function calculated numerically on a silo of width $100a$ with $\Delta=0.2$. The thin line is a typical response for a given realization of the disorder. Note that it takes negative values. The bold line has been averaged over 5000 realization of the disorder. The inset compares the averaged response peak with the one computed analytically, with a negative α. Note the negative part, as predicted by the theoretical calculation.

serving *negative* weights, which is, as we pointed out already, a structural property of the wave equation with randomness. Clearly, from a physical point of view, this is unacceptable and an additional rule should be added if the weight becomes locally negative. Some physically motivated rules could be invented (much as in [3]), but we do not want to pursue this here and leave this for future investigations.

In the present paper, we restrict to the case of a nonzero bare diffusion constant that, as argued above, should exist on a physical basis. Numerically, we have implemented this in two different ways.

The first one corresponds to letting the above scheme run until some height t_D and then start afresh with a regular lattice, where the forces are obtained by averaging over the nearest-neighbors belonging to the old lattice. This averaging procedure is clearly equivalent to a diffusion term. In this case, the numerical histograms do reach a stationary limit. We note that the total probability of negative forces is reduced when t_D is smaller; for $t_D\sim a$, the histogram is very nearly Gaussian around the average force; and for larger t_D, the tail of the probability distribution for large forces is of the form $\exp(-w^\beta)$, where $2>\beta>1$ (as found in [14]), where β is decreasing towards one as t_D increases, or for increasing disorder. For $t_D=10a$ and $\Delta=0.1$, we found $\beta\simeq 1.6$. The small force region has a much larger weight than found within the scalar model, although the presence of negative forces prevents us from being conclusive in this region.

The second scheme consists in simulating directly the three-leg model introduced above, with a random p chosen between 0 and p_M. These scheme is thus very close in spirit to the Liu *et al.* model. Again, the local forces are not everywhere positive and thus the small force region cannot be reliably studied. Nevertheless, the large force region behaves much in the same way as in the Liu *et al.* model. In particular, as shown in Fig. 18, the tail of the distribution decays as

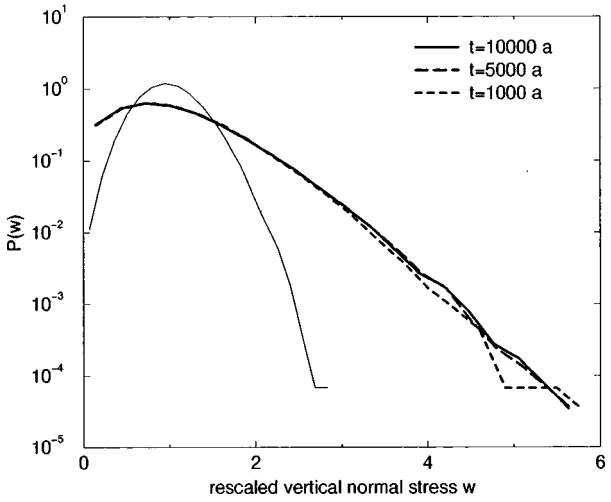

FIG. 18. These curves show the histograms of the vertical normal stress w, from which negative values have been removed. They all have been computed for the three-leg model, with periodic silos of width $1000a$. The three bold (solid, long-dashed, and short-dashed) lines are results from silos where the amplitude of the noise is maximum ($p_M=1$). The height of those silos is as indicated in the legend. The thin line represent a $1000a\times 1000a$ silo where the amplitude of the noise is $p_M=0.5$, where it is nearly Gaussian. Much like within the scalar model, $P(w)$ shows an exponential tail for large values of w when the disorder is maximum, while it is better fitted by a stretched exponential $\ln P(w)\sim -w^{\beta}$ with $\beta>1$, for smaller values of p_M.

$\exp(-w^{\beta})$ with $\beta\simeq 1$ when $p_M=1$ and with $\beta>1$ when $p_M<1$.

More work is needed to understand the physical implications of the presence of negative forces and any relation this may have to the static avalanche phenomenon [3]. However, the above results show that the tail of the force distribution is only exponential in a strong-disorder limit, where local arches (i.e., one grain entirely bearing on a single downward neighbor) have a nonzero probability.

VI. CONCLUSION

We have investigated in great detail the role of a local disorder in the propagation of stresses in granular media, both within a scalar approach, where only one component of the stress tensor is retained, and within the full tensorial approach, using a simple linear closure scheme [11,12], motivated partly by numerical simulations, which leads to a wavelike equation for stress propagation. The main effect of this local disorder is, in addition to introducing a diffusionlike term in the effective, large-scale equations, to renormalize the opening of the angle of the characteristic light cone for propagation of stress. Within a mode-coupling approximation scheme (exact for uncorrelated Gaussian noise), one finds that this angle vanishes for a critical disorder, beyond which stress propagates in a fundamentally different way (this regime might, however, not be physically relevant). The most striking difference between the scalar and tensorial approach is the fact that the response function becomes negative in the latter case, which is a source of instability of the packing to external perturbations. For moderate disorder, the response function takes negative values of order one near the point where the perturbation is applied and decays with distance. Hence we expect this instability to occur near the point where the perturbation is applied; at least near the upper surface of a pile under gravity, the effect occurs for a stress perturbation as small as the weight of one grain since this is sufficient to make the total local vertical stress negative.

Another difference that could be amenable to experimental verification is the structure of the correlation function, which gives direct information on how the information travels in the medium. Because of the analogy between the scalar model and passive scalar convection in turbulence, it is furthermore possible that higher moments of the correlation functions might reveal, in some circumstances, an intermittent behavior. Finally, the exponential falloff of the local stress distribution at high values, first found within the scalar model, also holds within a tensorial approach, but requires large disorder.

Several open points remain for further studies. First of all, we have considered only two-dimensional packings. The extension to three dimensions is rather straightforward: Although the structure of the response functions becomes inherently more complex in this case (see [10]), the main features discussed here (i.e., diffusive spreading and narrowing of the cone) are still valid.

Finally, we have not been able to determine analytically the histogram for local stresses within the random tensorial model. The major unsolved problem is the presence of negative forces, which induce a mechanical instability and imposes that an extra rule should be added to the stochastic wave equation to determine how stress propagates. As emphasized above, we believe that this is a direct consequence of the tensorial nature of the problem and can be interpreted as a signature of fragility of the contact network, which is generically unstable to very small perturbations [3,27].

ACKNOWLEDGMENTS

We thank V. Bucholtz, E. Clément, J. Duran, C. Eloy, and J. Rajchenbach for discussions, and A. Stott for a careful reading of the manuscript.

[1] R. L. Brown and J. C. Richard, *Principles of Powder Mechanics* (Pergamon, New York, 1966).

[2] L. Vanel, E. Clément, J. Lanuza, and J. Duran (unpublished).

[3] P. Claudin and J.-P. Bouchaud, Phys. Rev. Lett. **78**, 231 (1997).

[4] C.-h. Liu, S. R. Nagel, D. A. Scheeter, S. N. Coppersmith, S. Majumdar, O. Narayan, and T. A. Witten, Science **269**, 513 (1995).

[5] R. Brockbank, J. M. Huntley, and R. C. Ball, J. Phys. I. (to be published).

[6] D. M. Mueth, H. M. Jaeger, and S. R. Nagel (unpublished).
[7] G. W. Baxter, in *Powder and Grains 97*, edited by R. Behringer and J. T. Jenkins (Balkema, Rotterdam, 1997).
[8] See, e.g., P. Dantu (unpublished); Ann. Ponts Chaussées **4**, 193 (1967); T. Travers, *et al.* J. Phys. (Paris) **49**, 939 (1988).
[9] S. N. Coppersmith, C.-h. Liu, S. Majumdar, O. Narayan, and T. A. Witten, Phys. Rev. E **53**, 4673 (1996).
[10] J.-P. Bouchaud, M. E. Cates, and P. Claudin, J. Phys. I **5**, 639 (1995).
[11] J. P. Wittmer, M. E. Cates, P. Claudin, and J.-P. Bouchaud, Nature (London) **382**, 336 (1996).
[12] J. P. Wittmer, M. E. Cates, and P. Claudin, J. Phys. I **7**, 39 (1997).
[13] F. Radjai, M. Jean, J.-J. Moreau, and S. Roux, Phys. Rev. Lett. **77**, 274 (1996); F. Radjai, D. E. Wolf, M. Jean, and J.-J. Moreau, Phys. Rev. Lett. **80**, 61 (1998).
[14] C. Eloy and E. Clément, J. Phys. I **7**, 1541 (1997).
[15] M. Nicodemi, Phys. Rev. Lett. (to be published).
[16] M. Chertkov, G. Falkovich, and V. Lebedev, Phys. Rev. Lett. **76**, 3707 (1996), and references therein.
[17] M. Vergassola and A. Mazzino (unpublished).
[18] For a recent discussion on this approximation scheme and references see, e.g., J.-P. Bouchaud, L. Cugliandolo, J. Kurchan, and M. Mézard, Physica A **226**, 243 (1996).
[19] L. Saul, M. Kardar, and N. Read, Phys. Rev. A **45**, 8859 (1992); D. Cule and Y. Shapir, Phys. Rev. B **50**, 5119 (1994).
[20] S. F. Edwards and R. B. Oakeshott, Physica D **38**, 88 (1989); see also S. F. Edwards and C. C. Mounfield, Physica A **226**, 1 (1996); **226**, 12 (1996); **226**, 25 (1996).
[21] J. Smid and J. Novosad, Proceedings of the 1981 Powtech Conference [Ind. Eng. Chem. Symp. **63**, 1 (1981)].
[22] H. A. Janssen, Z. Vert. Dt. Ing. **39**, 1045 (1895); see also R. M. Nedderman, *Statics and Kinematics of Granular Materials* (Cambridge University Press, Cambridge, 1992).
[23] V. Bucholtz, J.-P. Wittmer, and M. E. Cates (unpublished).
[24] L. Landau and E. Lifshitz, *Elasticity Theory* (Pergamon, New York, 1986).
[25] O. Pouliquen (private communication).
[26] P.-G. de Gennes (private communication).
[27] In fact, fragility may arise even without disorder. The (noiseless) models of Refs. [10–12] predict that, in contrast to an elastic body, only certain combinations of boundary force can be supported by a given packing in static equilibrium; small deviations from these will cause a rearrangement of the contact network. See M.E. Cates, J.-P. Bouchaud, J.-P. Wittmer, and P. Claudin, in The Proceedings of Cargèse School ''Physics of Dry Granular Media,'' edited by H. Herrmann, J.-P. Hovi, and S. Luding (Kluwer Academic, Dordrecht, in press).